Low-Frequency Vibrations of *all-trans*-Retinal: Far-Infrared and Raman Spectra and Density Functional Calculations

Francesco Luigi Gervasio, Gianni Cardini, Pier Remigio Salvi, and Vincenzo Schettino*

Laboratorio di Spettroscopia Molecolare, Dipartimento di Chimica, Via Gino Capponi 9, 50121 Firenze, Italy, and European Laboratory for Nonlinear Spectroscopy (LENS), Largo E. Fermi 2, 50125 Firenze, Italy

Received: July 28, 1997; In Final Form: October 29, 1997

The infrared and Raman spectra of *all-trans*-retinal in the region of the low-frequency internal vibrations have been measured at room temeprature and at 15 K. The frequencies and infrared intensities of the normal modes have been calculated by means of the density functional approach using the B3-LYP exchange + correlation functional. The vibrational analysis allows a complete assignment of all the observed fundamentals, both on a frequency and on a intensity basis. The calculated vibrational modes of *all-trans*-retinal have been also correlated to those of the component moieties, 3,7-dimethyl-2,4,6,8-octatetraenal and 1,3,3-trimethyl-cyclohexene. This gives an idea of the degree of localization of the vibrational modes. It turns out that many of them are localized on the ring or on the chain fragment of the molecule. The chain torsional modes, which are of primary interest for the photoisomerization process, are correlated with torsional modes of bacteriorhodopsin.

Introduction

The infrared and Raman spectra of the retinal isomers have been the object of considerable interest from the theoretical[1−4] and experimental[5−12] point of view. Protein-bound retinals play the role of biological chromophores in rhodopsin and bacteriorhodopsin,[13] and the primary step in their photocycle is the isomerization of the retinal chromophore. The general approach to the vibrational spectroscopy of free and bound retinals has been to identify vibrational modes able to act as a probe and to monitor, through frequency shifts and intensity variations, structural, conformational, and environmental changes of the chromophore or of the protein.[13] However, the attention so far has mostly been confined to the middle infrared region (700−1600 cm^{-1}), and little is known about the low-frequency part of the spectrum. The latter can be of interest since the torsional motions around the C═C double bonds that are the relevant reaction coordinates in the primary isomerization process fall in this region. We felt it was useful, therefore, to investigate this low-frequency region of the spectrum in some detail as an attempt to enlarge the present knowledge of the vibrational structure of retinals. To this purpose, advantage can be taken of the approach to calculation of the vibrational frequencies based on density functional theory[14,15] that has been proved to be highly reliable in a number of medium sized molecules.[16] Extension of this approach to larger molecules, like the retinal isomers and their Schiff bases, can be useful.

The purpose of the present paper is to report and discuss the far-infrared absorption and the low-frequency Raman scattering of *all-trans*-retinal whose molecular structure is represented in Figure 1. The spectra of the solid have been obtained both at room and low temperature. With the help of the density functional calculation[14,15] of the vibrational frequencies[17] and of the infrared intensities, the assignment of all the low-frequency internal modes is discussed. The results are compared with the low-frequency data on bacteriorhodopsin[18] and rhodopsin[19] to support the correctness of our conclusions.

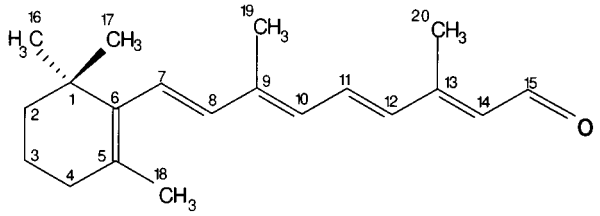

Figure 1. The molecular structure of *all-trans*-retinal.

Experimental Section

all-trans-Retinal (>98% purity) from Sigma Aldrich was stored in the dark at −20 °C and used without further purification. Samples of *all-trans*-retinal as a pure pellet and in a polythene matrix were prepared for infrared measurements (700−30 cm^{-1}) in half-light conditions and quickly transferred in the spectrometer or on the coldfinger of the cryostat. Less frequently, spectra were measured down to 200 cm^{-1} with *all-trans*-retinal as a polycrystalline film between CsI windows. The measurements were always done on freshly prepared samples. No appreciable variation of band shapes in the course of the experiments was noticed. Spectra identical with previous reports[5,6] were also run in the mid-infrared region (1800−500 cm^{-1}). A FTIR spectrometer (Bruker mod. IFS 120 HR), operating with a Mylar beam splitter and with a bolometer cooled at liquid He temperature as the detector, was used for the far-infrared experiments. The spectral resolution was 0.5−1 cm^{-1}, much lower in all cases than the observed bandwidths. Low-temperature spectra were obtained by cooling at 15 K the sample placed on the finger of a closed circuit He cryostat.

Raman spectra were measured in a backscattering geometry with both a FT-Raman Bruker interferometer, using as the exciting line the Nd: YAG laser emission at 1064 nm, and a conventional Raman instrument equipped with a Jobin-Yvon double monochromator (spectral resolution ≃ 1 cm^{-1}), a red-extended photomultiplier (RCA mod. C31034A), a photon counting detection system, and a PC for data processing and

S1089-5639(97)02463-8 CCC: $15.00
Published on Web 02/27/1998

TABLE 1: Calculated (6-31G* Basis Set; Density Functional Calculation) and Experimental Bond Lengths (Å) of the Polyenic *all-trans*-Retinal Chain[a]

	calc[b]		expt[c]
C_5-C_6	1.358	1.370	1.329
C_6-C_7	1.474	1.451	1.483
C_7-C_8	1.354	1.366	1.317
C_8-C_9	1.455	1.441	1.469
C_9-C_{10}	1.368	1.381	1.346
$C_{10}-C_{11}$	1.436	1.422	1.443
$C_{11}-C_{12}$	1.361	1.372	1.339
$C_{12}-C_{13}$	1.451	1.437	1.455
$C_{13}-C_{14}$	1.366	1.379	1.346
$C_{14}-C_{15}$	1.459	1.440	1.458
$C_{15}-O$	1.223	1.255	1.201

[a] See Figure 1 for atom numbering. [b] First column, this work; second column, data from ref 1 (density functional calculation in the local density approximation). [c] From ref 22.

exciting with the 647.1 nm line of a Kr laser. The mildly compressed pure sample was placed in the hollow cavity of a metallic holder, attached, in the case of low-temperature experiments, to the coldfinger of a cryostat. The low power, $\simeq$ 20 mW, exciting beam strikes unfocused on the crystal powder to avoid sample deterioration. The sample stability with respect to irradiation was also checked by measuring the Raman spectrum at room temperature, then cooling the sample, and finally measuring the room temperature spectrum again. The initial and final spectra were identical. No effect was noticed on the Raman intensities when the exciting line or the laser power were changed. The FT-Raman spectra were taken only at room temperature.

Calculations

Calculations of the structure, vibrational frequencies and infrared intensities of *all-trans*-retinal were carried out with ab initio MO methods within the density functional approach using the GAUSSIAN 94[20] package. The calculation included a preliminary study of a series of smaller molecules, such as *all-trans* polyenes $CH_2-(CH=CH)_n-CH_2$ ($n = 2-5$), the two methylated derivatives (2,6-dimethyl-1,3,5,7-octatetraene and 3,7-dimethyl-2,4,6,8-octatetraene), and the cyclic system 1,3,3-trimethylcyclohexene, to check the reliability of the calculation method. The results will be discussed in detail separately.[21] In the present paper we will only be concerned with data on *all-trans*-retinal. We only mention that the calculation was performed with the split valence polarized 6-31G* basis set and that the B3-LYP density functional was used. This is a mixed functional of the generalized gradient approximation (GGA) type including the Becke (B3) exchange[14] and the Lee, Yang, and Parr (LYP)[15] correlation functionals. The numerical integration of the electronic density is over a grid of 75×434 points around each atom. As we are mainly interested in vibrational frequencies, a recent comparative analysis[17] of calculated vibrational frequencies on 122 molecules using five different density functionals has shown that the best results (in terms of smallest root-mean-square differences between experimental and calculated frequencies) are obtained with the B3-LYP functional.

The equilibrium structure of the isolated *all-trans* molecule has been calculated, and some relevant structural parameters are reported in Table 1. The agreement with experimental data[22] is satisfactory and appreciably better than in recent ab initio calculations.[1]

For the calculation of the vibrational frequencies, second derivatives were obtained by analytical methods to avoid finite incremental step size errors arising in numerical differentiation. The calculated harmonic frequencies were scaled using the optimum uniform scaling factor of 0.9613.[17] The scaling factor empirically corrects for the anharmonicity of the molecular vibrations. Calculation on the simpler molecules (*all-trans* polyenes $CH_2-(CH=CH)_n-CH_2$ ($n = 2-5$)) and comparison between calculated and observed frequencies[21] show that by using the proposed scaling factor[17] the calculated frequencies above 1000 cm^{-1} are still higher than the experimental frequencies, the difference decreasing with decreasing frequency. This shows that the empirical anharmonic correction ensured by the scaling factor in this region is not sufficient. On the contrary, it has been found[21] that in the low-frequency region the scaling factor is such as to produce calculated frequencies generally smaller than experimental frequencies. This occurs also in the retinals as can be seen from Table 2. No attempts have been made to work out a frequency-dependent scaling factor.

Results and Vibrational Assignment

The far-infrared spectrum of *all-trans*-retinal between 700 and 30 cm^{-1} at room temperature is shown in Figure 2. Four main absorption bands are observed centered at 487, 409, 162, and 43 cm^{-1}. These and a number of other bands of medium/weak intensity appear to have an unresolved structure at room temperature. In the same figure the calculated spectrum is reported with all vibrational transitions convoluted with a Lorentzian profile of width 20 cm^{-1} to simulate room temperature bandwidths. A good correspondence can be established between the two traces. In particular, the strongest bands (487, 409, 162 cm^{-1}) are well reproduced both in frequency and relative intensity. The intensity of the 43 cm^{-1} band is slightly underestimated. The calculated intensities result from the contribution of several close-lying vibrational modes. All other calculated bands are weaker, as observed experimentally. The infrared spectrum at 15 K is reported in Figure 3. Experimental data are collected in Table 2 with the vibrational assignment.

The Raman spectra at room and low temperature are shown in Figure 4. The room temperature spectrum has already been reported though not discussed in detail.[23] The remarkable relative intensities of the 32 and 48 cm^{-1} Raman peaks can be noted. As already pointed out,[23] most of the lowest frequency features are common to all retinal isomers, strongly suggesting their assignment to intramolecular modes. The spectral changes as a function of temperature closely resemble those observed in the infrared spectrum. Band maxima shift to higher frequencies on lowering the temperature, the effect being particularly evident for low-frequency bands, which also split into several components. At low temperature a broad continuum band develops in the Raman spectrum with its maximum around $\approx$1500 cm^{-1} from the exciting line. This band has been subtracted in the spectrum of Figure 4. Upon warming the sample the broad feature disappears. The origin of the band is unknown and can be tentatively related to an emission either from impurities or from the bulk crystal following a strongly red-shifted electronic absorption. Unfortunately, the low-temperature FT-Raman spectrum is not available to rule out this explanation.

The substantial agreement between calculated and observed infrared spectra at room temperature allows us to attempt a complete assignment of the infrared and Raman spectra. The analysis, summarized in Table 2, has been made on the basis of the following remarks. Possible solid-state effects on the observed spectra should be considered. *all-trans*-Retinal crystallizes in the monoclinic system, space group C^5_{2h} ($P_{2_1/n}$), with

TABLE 2: Observed Infrared and Raman Frequencies (cm^{-1}) and Intensities (*I*) of *all-trans*-Retinal and Frequencies (cm^{-1}) Calculated with the B3-LYP Density Functional Approach of *all-trans*-Retinal and Component Moieties[a]

obs						calc			
IR			Raman			R	r	c	
ω[b]		I[c]	ω[b]		I[c]	ω			assign.[d]
{652	652		655	657	w	637		634	chain bending ($C_{11}C_{12}C_{13}$; $C_{13}C_{14}C_{15}$; $C_{13}C_{20}$ H)
{650	650								
641			640						hot band
623	625	m	628	629	w	617			ring torsion ($C_1C_6C_5C_4$) + chain bending ($C_7C_8C_9$; $C_{11}C_{12}C_{13}$)
601	602	mw	600	603	w	586		567	chain bending ($C_9C_{10}C_{11}$; $C_{10}C_9C_{19}$)
581	581	w	587	587	vw	559	565		ring stretching (C_1C_6; C_5C_{18}) + bending ($C_3C_4C_5$)
540	541	ms	543			532		532	chain torsion ($C_{10}C_{11}C_{12}C_{13}$) + wagging ($C_{12}C_{13}C_{14}-C_{20}$)
531	531	s	530			518			ring bending ($C_5C_6C_7$) + chain wagging ($C_8C_9C_{10}-C_{19}$)
	502	vw	502	504	w	488			ring bending ($C_1C_6C_5$; $C_2C_3C_4$) + chain bending ($C_{12}C_{13}C_{14}$)
{491	490					483		462	chain bending ($C_8C_9C_{10}$) + wagging ($C_8C_9C_{10}-C_{19}$)
{487	486								
481	482	s	480	481	m	466			chain bending ($C_8C_9C_{10}$; $C_{12}C_{13}C_{14}$) + ring bending ($C_2C_1C_{17}$)
466	466	w	470			456			chain ($C_2C_1C_6$; $C_3C_4C_5$) + ring bending ($C_6C_7C_8$; $C_8C_9C_{19}$; $C_{12}C_{13}C_{14}$)
431	430	w	430			420	442		ring bending ($C_4C_5C_{18}$ + $C_2C_1C_{16}$)
	414	s	413	416	m	405	389		ring torsion ($C_3C_4C_5C_6$) + bending ($C_2C_1C_{17}$) + CH_2 rocking
409	408	s				395		387	methyl chain bending ($C_8C_9C_{19}$; $C_{12}C_{13}C_{20}$)
377	382	w	383	384	vw	372	393		ring bending ($C_2C_1C_{17}$) + CH_2 rocking
369	372	m	370	374	vw	358			chain torsion ($C_7C_8C_9C_{10}$; $C_8C_9C_{10}C_{11}$) + methyl ring bending ($C_6C_5C_{18}$)
343	344	w				337			ring ($C_1C_6C_5$) and chain ($C_{12}C_{13}C_{20}$) bending + chain torsion ($C_8C_9C_{10}C_{11}$)
331	334	br	330		vw	325			ring bending ($C_2C_1C_{16}$; $C_{16}C_1C_{16}$) + chain torsion ($C_8C_9C_{10}C_{11}$)
			310	{312	m	305	317		ring bending ($C_{16}C_1C_{17}$)
				{314	sh				
301	304	mw				290		283	chain bending ($C_{10}C_9C_{19}$; $C_{10}C_{11}C_{12}$; $C_{13}C_{14}C_{15}$)
	290	br	290			301			ring ($C_{16}C_1C_{17}$) + chain ($C_{14}C_{13}C_{20}$) bending
						258	280		ring torsion ($C_3C_4C_5C_6$)
	260	vw		265		256		257	terminal chain torsion ($C_{11}C_{12}C_{13}C_{14}$; $C_{12}C_{13}C_{14}C_{15}$)
	240	w			w	252	252		methyl ring torsion (C_1-C_{17} H_3)
221	231	m		225	m	234			chain bending ($C_8C_9C_{19}$) + methyl ring torsion (C_5-C_{18} H_3)
205	215	w	207	217	m	218	239		methyl ring torsion (C_1-C_{17} H_3;C_5-C_{18} H_3)
	194	w				205	230		methyl ring torsion (C_1-C_{16} H_3)
180	184	m		181	w	184		188	terminal chain torsion ($C_{12}C_{13}C_{14}C_{15}$; $C_{13}C_{14}C_{15}$O)
	172	s				172			ring torsion (C_1-C_{17} H_3) + chain torsion ($C_{13}C_{14}C_{15}$ O)
162	163	s	165			164		169	methyl chain torsion ($C_{13}-C_{20}$ H_3)
				157	s	155			chain methyl (C_9-C_{19} H_3) + ring (C_5-C_{18} H_3) torsion
	152	s	147	151	s	151		151	methyl chain torsion (C_9-C_{19} H_3)
127	130	m			m	143		135	methyl chain torsion (C_9-C_{19} H_3; $C_{13}-C_{20}$ H_3)
			117	121	m	115	126		ring torsion ($C_1C_6C_5C4$); ($C_1C_6C_5C_{18}$)
				112	sh				?
103	109	m	96	105	s	99	101		ring torsion ($C_2C_1C_6C_5$)
82	89	s	74	81	vw	110		105	chain ($C_9C_{10}C_{11}C_{12}$; $C_{12}C_{13}C_{14}C_{15}$) torsion
	68	w	58	73	m	78			chain torsion ($C_6C_7C_8C_9$) + ring bending ($C_5C_6C_7$)
				70	sh				?
	64	sh							?
	53	m	58	54	s	59			ring torsion ($C_2C_1C_6C_5$; $C_4C_5C_6C_7$) + chain bending ($C_{10}C_{11}C_{12}$)
43	46	m	48	44	s	49		55	terminal chain torsion ($C_{10}C_{11}C_{12}C_{13}$; $C_{11}C_{12}C_{13}C_{14}$)
			32	38	s	35		36	terminal chain torsion ($C_{10}C_{11}C_{12}C_{13}$; $C_{11}C_{12}C_{13}C_{14}$)
				34	sh	29			relative chain/ring bending ($C_6C_7C_8$; $C_{10}C_{11}C_{12}$)
						17			relative chain/ring torsion ($C_1C_6C_7C_8$; $C_9C_{10}C_{11}C_{12}$; $C_7C_8C_9C_{10}$)

[a] R = *all-trans*-retinal; c, Chain = 3,7-dimethyl-2,4,6,8-octatetraenal; r, Ring = 1,3,3-trimethylcyclohexene. [b] Room and low-temperature frequencies in the first and second column, respectively. [c] Intensities (*s* = strong, m = medium, w = weak, sh = shoulder, br = broad) refer to the low-temperature spectra. [d] Approximate description of each normal mode on the basis of the potential energy distribution among internal coordinates. With reference to atomic numbering of Figure 1, $C_nC_mC_l$ stands for bending between *n*, *m*, *l* carbon atoms, $C_nC_mC_lC_k$ for torsion between *n*, *m*, *l*, *k* carbon atoms and $C_nC_mC_l-C_k$ for out-of-plane bending (wagging) of the *k*-th atom with respect to the *n*, *m*, *l* plane.

four molecules per unit cell.[22] Each normal mode of the isolated molecule splits in the crystal into 4 components, two Raman (symmetry species a_g and b_g) and two infrared active (symmetry species a_u and b_u). Therefore, the infrared and Raman frequencies may differ by few wavenumbers as an effect of the factor group splitting. In addition, in the region below ≈100 cm^{-1} 21 lattice vibrational modes occur, classified as $5a_u + 4b_u + 6a_g + 6b_g$. These will be coupled to the low-frequency molecular vibrations. However, only six internal modes of *all-trans*-retinal are calculated at frequencies below 100 cm^{-1}, and therefore the intermolecular forces and the coupling to lattice modes will affect only a small portion of the spectra discussed in this work. It can be noted in Table 2 that some of the observed frequencies below 100 cm^{-1} are unassigned and they should likely be identified as librational or translational modes of the whole molecule.

A simplified description of the vibrational modes is included in the last column of Table 2. This has been obtained from the potential energy distribution.[24] In some cases the assignment has been confirmed by comparing the calculated frequencies of *all-trans*-retinal with those of species with selected isotopic substitution. A correlation between the calculated frequencies of *all-trans*-retinal and those of the two moieties (3,7-dimethyl-2,4,6,8-octatetraenal and 1,3,3trimethylcyclohexene) is also

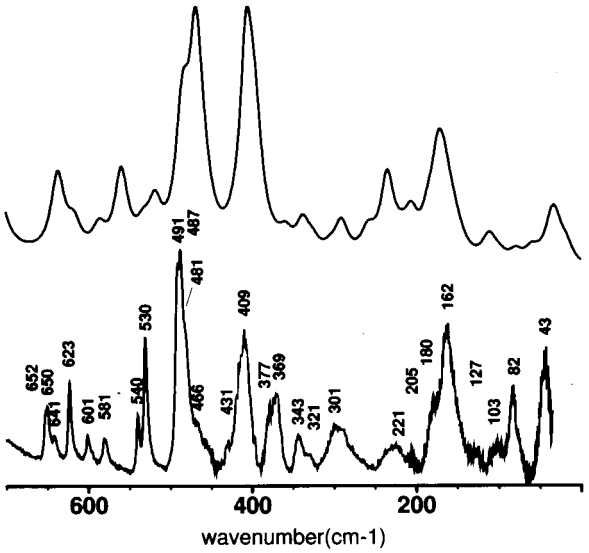

Figure 2. (lower) Room temperature infrared spectrum of *all-trans*-retinal in a polythene (450−30 cm^{-1}) and in a KBr (700−450 cm^{-1}) pellet. (upper) Calculated spectrum using density functional results of vibrational frequencies and intensities (see text for details) and convoluting with Lorentzian profiles (bandwidth 20 cm^{-1}).

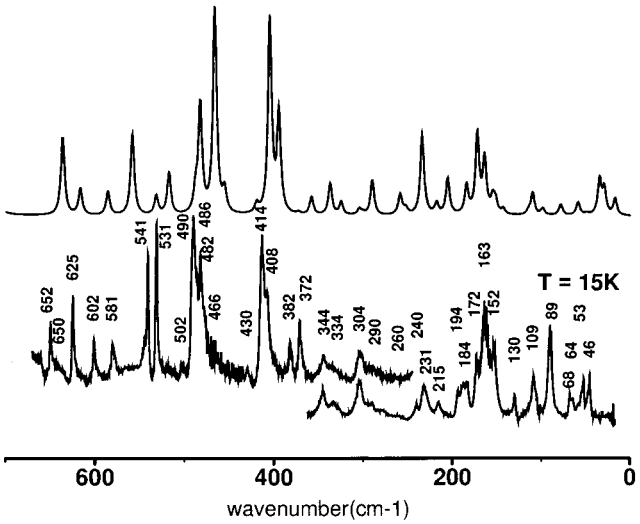

Figure 3. (lower) Infrared spectrum of *all-trans*-retinal in a polythene pellet at 15 K in the vibrational region 700−30 cm^{-1}. (upper) Calculated spectrum using density functional results of vibrational frequencies and intensities (see text for details) and convoluting with Lorentzian profiles (bandwidth 5 cm^{-1}).

included in Table 2. This gives an idea of the degree of localization of the vibrational motions on one part or the other of *all-trans*-retinal. It can be noted that while several frequencies are little changed when the two moieties are bound in the retinal, others are quite different, indicating the collective character of these modes. This character is particularly evident for the lowest frequency modes that have no counterpart in any of the moieties.

It is useful to illustrate the vibrational assignment summarized in Table 2 in the various spectral regions. In the 650−500 cm^{-1} region six vibrational modes with medium infrared intensity are calculated, in good agreement with the observed infrared (650/652, 625, 601, 581, 540, 531 cm^{-1}) and Raman peaks (657, 629, 603, 587, 543, 530 cm^{-1}). A band at 641 cm^{-1} in both spectra at room temperature disappears at 15 K and is accordingly interpreted as a hot band. These modes are combinations of CCC bending and CCCC torsion and wagging motions,

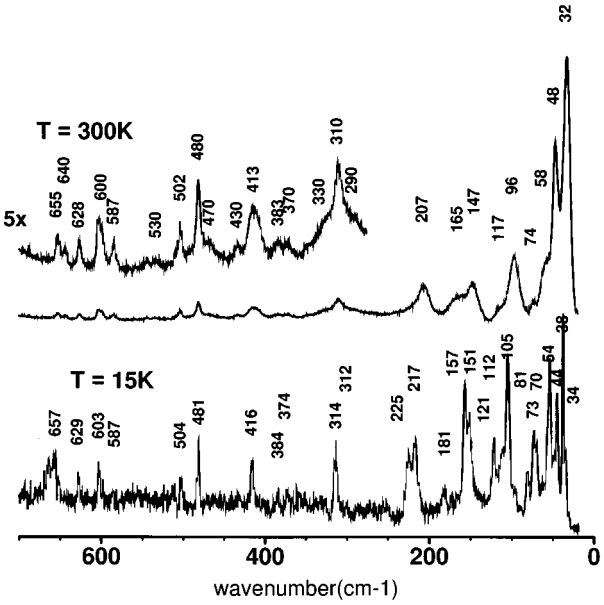

Figure 4. The Raman spectra (λ_{exc} = 647.1 nm) of polycrystalline *all-trans*-retinal at room temperature (upper) and at 15 K (lower).

localized on the ring (calc, 559 cm^{-1}), on the chain (calc, 637, 586, 532 cm^{-1}), or of mixed character (calc, 617, 518 cm^{-1}). In particular, it should be noted that the two lowest, 540(IR)/543(Raman) cm^{-1} and 531(IR)/530(Raman) cm^{-1}, assigned as vibrations of predominantly torsional/wagging and bending/wagging character, respectively, give rise to relatively large oscillating dipoles and show in the infrared but are very weak in the Raman spectrum.

At lower frequencies four vibrational modes are calculated at 488, 483, 466, and 456 cm^{-1} of mixed chain-ring character (except the second, localized on the chain) and involving mostly CCC bending coordinates. On the basis of the calculated infrared intensities, the two strongest modes (483 and 466 cm^{-1}) are assigned to the 490/486 cm^{-1} crystal doublet and to the 482 cm^{-1} singlet, respectively, and the two weakest to the side peaks 502, 465 cm^{-1}. The room temperature 409 cm^{-1} infrared peak is resolved at 15 K into a triplet (430, 414, 408 cm^{-1}), comparing nicely with the calculated modes at 420, 405, and 395 cm^{-1}. The first mode, 420 cm^{-1}, is a $C_4C_5C_{18} + C_2C_1C_{16}$ ring bending while the other two are approximately a ring torsion and a chain bending, respectively.

From the latter group of bands to the next of comparable intensity around 162 cm^{-1}, nine medium/weak peaks are distinctly observed with three additional weaker bands. In good agreement with experiment, 13 modes are calculated in this region. The Raman frequencies correlate fairly well with the infrared, apart from the 312/314 cm^{-1} medium intensity crystal doublet. This latter is assigned as the missing fundamental in this region. The assignment of the 231 (a mixed chain bending and methyl ring torsion mode) and of the 184 cm^{-1} (a torsional mode localized on the chain terminal atoms) peaks is straightforward, comparing with the calculated frequencies and infrared intensities. The same can be said for the three doublets observed at 382−372, 344−334, and 290−304 cm^{-1} on the basis of observed and calculated relative intensities. It can be noted that modes with a large torsional contribution from the chain (372, 344, 184 cm^{-1}) have a more pronounced infrared than Raman activity. A fourth similar torsional mode (265 cm^{-1}) is very weak (or absent) both in the infrared and Raman spectrum. Almost pure torsions of the ring methyls are assigned at 240, 215, and 194 cm^{-1}.

TABLE 3: Calculated Frequencies (cm^{-1}) of the Methyl Torsional Vibrations in *all-trans*-Retinal-d_0 and -d_3 Derivatives

retinal-d_0	retinal-d_3	isotopic substitution[a]
205	149	met16
252	162	met17
155	132	met18
151	118	met19
164	119	met20

[a] See Figure 1.

In the region just above 150 cm^{-1}, a room temperature infrared band splits into three components at 15 K. A fourth peak, 157 cm^{-1}, is observed in the Raman spectrum. The four bands are assigned as torsions of the chain methyl groups (163 and 151 cm^{-1}) and as chain and ring torsions (172 and 157 cm^{-1}).

The assignment of the modes below 150 cm^{-1} is more difficult mainly because of the overlap and mixing with the translational and librational modes of the whole molecules occurring in the same region. The tentative assignment reported in Table 2 was made assuming that one mode is observed only in the infrared and two modes only in the Raman spectrum. It is also assumed that the 32 and 48 cm^{-1} Raman bands are due to intramolecular vibrations and that the lattice modes do not exceed 70 cm^{-1}. The latter hypothesis is reasonable considering the mass and inertia moments of the retinal. Only the lowest calculated frequency (17 cm^{-1}) is left unassigned.

It can be seen from Table 2 that above 200 cm^{-1} a large number of normal modes are localized on the chain or ring retinal moieties. Below this frequency, on the contrary, the modes develop as collective motions of the molecules with a poor degree of localization. The effect of deuterium substitution on the methyl groups is reported in Table 3. This confirms the assignment of the methyl torsion vibrations obtained from the potential energy distribution. These normal modes appear therefore pretty well localized. An attempt to identify more clearly the C−C−C−C torsional vibrations of the chain has been made with the help of $^{13}C-^{12}C$ isotopic substitution on these atoms. However, this affects the frequencies of the bending modes as well. It is evident from the potential energy distribution and the effect of isotopic substitution that the torsional modes are strongly coupled each with the other and to a smaller extent also with the bending modes. The isotopic substitution allows us to roughly identify torsional modes at 532, 358, 337, 256, and 184 cm^{-1}, as summarized in Table 2.

Discussion

Since the low-frequency infrared and Raman spectra of *all-trans*-retinal have not been reported so far, direct comparison with previous results is not possible. However, there is some information available on bacteriorhodopsin (BR) where *all-trans*-retinal is bound to the Lys-216. Low-frequency BR modes have been observed in a resonance Raman experiment (568 nm, excitation line)[18] at 557, 529, 497, 452, 402, 284, 266, and 187 cm^{-1}. Comparing the spectrum of bacteriorhodopsin[18] with our and the reported[5,6] spectra of *all-trans*-retinal in the fingerprint and out-of-plane regions, it may be concluded that Raman modes change only moderately going from the free to the bound chromophore. Reasonably, this holds also for low-frequency modes. In fact, the Raman modes 543, 530, 502, 480, 413, 290, 265, and 181 cm^{-1} of the *all*-trans isomer should correspond to previous reported BR peaks.[18] It can be noted that the modes of BR corresponding to the three modes of *all-trans*-retinal at 543, 265, and 181 cm^{-1} are resonantly intensified. From the vibrational assignment discussed above, it can be seen that these three modes are actually pure or predominant torsions, calculated at 532, 256, and 184 cm^{-1}. A few torsional modes are schematically depicted in Figure 5. The normal displacements justify satisfactorily the medium infrared activity of the 532 and 184 cm^{-1} modes and the inactivity of the 256 cm^{-1} mode. The first, 532 cm^{-1}, is mostly located on the $C_{12}H-C_{13}-C_{14}H$ molecular fragment, developing an oscillating dipole normal to the polyene plane. This is substantially true also for the more complex 184 cm^{-1} vibration. Conversely, the 256 cm^{-1} coordinate has contributions to the electric dipole almost canceling each with the other and, as a consequence, vanishing infrared intensity. On the contrary, the three peaks 502, 480, and 413 cm^{-1} (497, 452, and 402 cm^{-1}, corresponding BR values) have approximately the same relative intensities in the two spectra. Only bending modes have been found by our calculations in the 500−400 cm^{-1} region. In particular, the first two have been assigned as mixed ring and chain bendings and the third as ring torsion + bending.

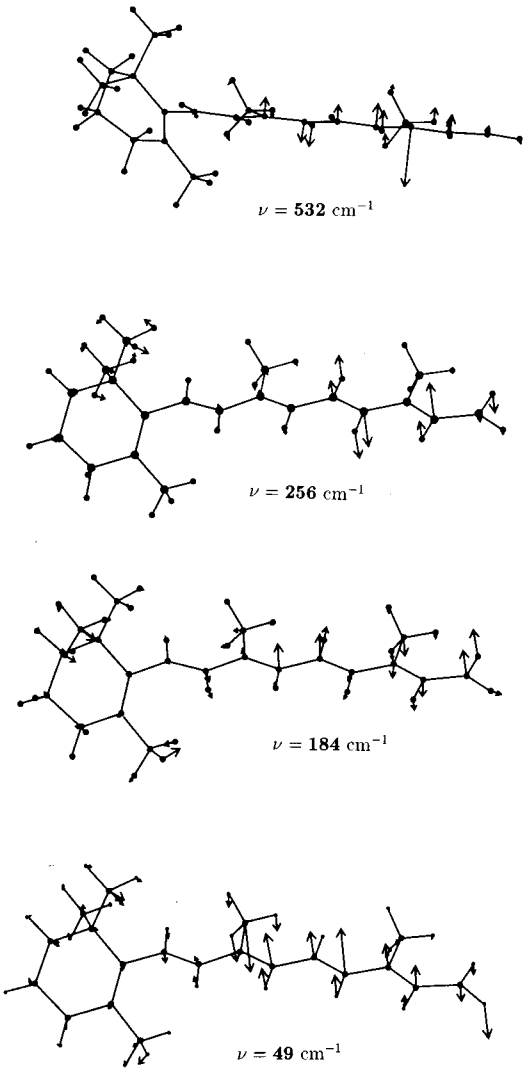

Figure 5. Atomic displacements of selected torsional modes (532, 256, 184, 49 cm^{-1}) of *all-trans*-retinal obtained by the density functional calculation.

With due caution the analysis may be extended to the low-frequency Raman spectrum of rhodopsin (RH).[19] Here the chromophore is 11-*cis*-retinal and the vibrational calculation of *all-trans*-retinal may not be appropriate. Nevertheless, experi-

mental similarities exist.[18,19] A prominent band is seen at 262 cm^{-1} and a weaker one at 461 cm^{-1}. It is tempting to assume that the 266 cm^{-1} BR and the 262 cm^{-1} RH modes come from similar torsional coordinates. As it is seen from Figure 5, the 256 cm^{-1} mode is localized on the terminal chain portion and independent to a first approximation on the *cis/trans* geometry around the C_{11}═C_{12} double bond.

Finally, it is worth noting that in a femtosecond study on the photoisomerization of rhodopsin a coherent 60 cm^{-1} oscillation of the *all-trans* photoproduct has been identified,[25] originating from a skeletal torsional mode of the chromophore and with a large projection along the C_{11}═C_{12} torsional mode. This mode should likely correspond to that of *all-trans*-retinal calculated at 49 cm^{-1}, which, however, appears as a collective mode of the chain rather than a torsion with appreciable degree of localization. The same torsional mode, calculated at 56 cm^{-1} with semiempirical methods,[4] has been shown to be responsible for the vibronic structure of the *all-trans*-retinal $S_0 \rightarrow S_1$ absorption spectrum.

Conclusions

The low-frequency modes of *all-trans*-retinal have been observed by means of infrared and Raman spectroscopy and assigned by comparison with vibrational calculations based on density functional theory. Vibrations of *all-trans*-retinal have been correlated to those of ring and chain moieties, showing that they are in many cases localized on one or the other part of the molecule. This is the first report of an ab initio calculation on the low frequency modes of a retinal isomer. Recently an ab initio molecular dynamics calculation has been reported,[1] but only few vibrational modes falling in the mid-infrared region have been discussed. Previous calculations on retinals were carried out on model molecules,[5,6] but the low-frequency results were not reported. A full semiempirical calculation has been reported by Warshel et al. using the QCFF-PI approach.[4,26] The semiempirical results differ appreciably from the ab initio calculation in the mid-infrared region, but the two types of calculation compare reasonably in the low-frequency region. The present calculation and the good agreement between calculated and observed infrared spectra show that the density functional approach is quite effective for this type of molecule. Calculations are presently in progress in our laboratory on the retinal isomers and their Schiff bases.

Acknowledgment. The authors gratefully acknowledge the help of Dr. R. Bini for far-infrared measurements. This work was supported by the Italian Consiglio Nazionale delle Ricerche (CNR), by the Ministero dell′Università e della Ricerca Scientifica e Tecnologica (MURST), and by the E.U. under the Contract ERBFMGECT950017.

References and Notes

(1) Bifone, A.; de Groot, H. J. M.; Buda, F. *Chem. Phys. Lett.* **1996**, *248*, 165.
(2) Grossjean, M. F.; Tavan, P.; Schulten, K. *J. Phys. Chem.* **1990**, *94*, 8059.
(3) Birge, R. R.; Bocian, D. F.; Hubbard, L. M. *J. Am. Chem. Soc.* **1982**, *104*, 1196.
(4) Warshel, A.; Karplus, M. *J. Am. Chem. Soc.* **1974**, *96*, 5677.
(5) Curry, B.; Broek, A.; Lugtenburg, J.; Mathies, R. A. *J. Am. Chem. Soc.* **1982**, *104*, 5274.
(6) Saito, S.; Tasumi, M. *J. Raman Spectrosc.* **1983**, *14*, 236.
(7) Cookingham, R. E.; Lewis, A. *J. Mol. Biol.* **1978**, *119*, 569.
(8) Rimai, L.; Gill, D.; Parsons, J. L. *J. Am. Chem. Soc.* **1971**, *93*, 1353.
(9) Inagaki, F.; Tasumi, M.; Miyazawa, T. *J. Raman Spectrosc.* **1975**, *3*, 335.
(10) Mathies, R. A.; Smith, S. O.; Lugtenburg, J. *Biophysical Studies of Retinal Proteins;* University of Illinois Press: Urbana, IL, 1987.
(11) Siebert, F. In *Biomolecular Spectroscopy, Part A*; Clark, R. J. H., Hester, R. E., Eds.; J. Wiley and Sons: New York, 1993.
(12) Mathies, R. A.; Smith, S. O.; Palings, I. In *Biological Applications of Raman Spectroscopy*; Spiro, T., Ed.; J. Wiley and Sons: New York, 1987.
(13) Birge, R. R. *Biochim. Biophys. Acta* **1990**, *1016*, 293.
(14) Becke, A. D. *Phys. Rev. A* **1988**, *33*, 3098.
(15) Lee, C.; Yand, W.; Parr, R. G. *Phys. Rev. B* **1988**, *37*, 785.
(16) Ziegler, T. *Chem. Rev.* **1991**, *91*, 651.
(17) Wong, M. W. *Chem. Phys. Lett.* **1996**, *256*, 391.
(18) Myers, A. B.; Harris, R. A.; Mathies, R. A. *J. Chem. Phys.* **1983**, *79*, 603.
(19) Loppnow, G. R.; Mathies, R. A. *Biophys. J.* **1988**, *54*, 35.
(20) Frisch, M. J.; Trucks, G. W.; Schlegel, H. B.; Gill, P. M. W.; Johnson, B. G.; Robb, M. A.; Cheeseman, J. R.; Keith, T.; Petersson, G. A.; Montgomery, J. A.; Raghavachari, K.; Al-Laham, M. A.; Zakrzewski, V. G.; Ortiz, J. V.; Foresman, J. B.; Cioslowski, J.; Stefanov, B. B.; Nanayakkara, A.; Challacombe, M.; Peng, C. Y.; Ayala, P. Y.; Chen, W.; Wong, M. W.; Andres, J. L.; Replogle, E. S.; Gomperts, R.; Martin, R. L.; Fox, D. J.; Binkley, J. S.; Defrees, D. J.; Baker, J.; Stewart, J. P.; Head-Gordon, M.; Gonzalez, C.; Pople, J. A. *Gaussian 94, Revision D.3;* Gaussian Inc.: Pittsburgh, PA, 1995.
(21) Gervasio, F. L.; Cardini, G.; Salvi, P. R.; Schettino, V. In preparation.
(22) Hamanaka, T.; Mitsui, T.; Ashida, T.; Karudo, M. *Acta Crystallogr.* **1972**, *B28*, 214.
(23) Cookingham, R. E.; Lewis, A.; Lemley, A. T. *Biochemistry* **1978**, *17*, 4699.
(24) A more detailed description of the calculated normal modes in terms of potential energy distribution is available, on request, from the authors.
(25) Wang, Q.; Schoenlein, R. W.; Peteanu, L. A.; Mathies, R. A.; Shank, C. V. *Science* **1994**, *266*, 422.
(26) Warshel, A.; Dauber, M. *J. Chem. Phys.* **1977**, *66*, 5477.